Evolution of Solute-Water Interactions in the Benzaldehyde-(H2O)1-6 Clusters by Rotational Spectroscopy

Journal:	*Journal of the American Chemical Society*
Manuscript ID	ja-2022-11732p.R3
Manuscript Type:	Article
Date Submitted by the Author:	28-Jan-2023
Complete List of Authors:	Li, Weixing; Fudan University Pérez, Cristóbal; University of Valladolid, Physical Chemistry Steber, Amanda; Deutsches Elektronen-Synchrotron Schnell, Melanie; Max-Planck-Institut fur Struktur und Dynamik der Materie, DESY Lv, Dingding; Fudan University, Chemistry Wang, Guanjun; Fudan University, Chemistry Zeng, Xiaoqing; Fudan University, Department of Chemistry Zhou, Mingfei; Fudan University, Chemistry

Evolution of Solute-Water Interactions in the Benzaldehyde-$(H_2O)_{1-6}$ Clusters by Rotational Spectroscopy

Weixing Li,[a]* Cristóbal Pérez,[b†] Amanda L. Steber,[b†] Melanie Schnell,[b,c]* Dingding Lv,[a] Guanjun Wang,[a] Xiaoqing Zeng,[a] Mingfei Zhou[a]*

[a]Department of Chemistry, Shanghai Key Laboratory of Molecular Catalysis and Innovative Materials, Fudan University, Songhu Rd. 2005, 200438 Shanghai, China.

[b]Deutsches Elektronen-Synchrotron DESY, Notkestraße 85, 22607 Hamburg, Germany.

[c]Christian-Albrechts-Universität zu Kiel, Institute of Physical Chemistry, Max-Eyth-Str. 1, 24118 Kiel, Germany.

[†]Present address of Dr. Cristóbal Pérez, and Dr. Amanda Steber:

Departamento de Química Física y Química Inorgánica, Facultad de Ciencias-I.U. CINQUIMA, Universidad de Valladolid, E-47011 Valladolid, Spain.

*Corresponding authors: weixingli@fudan.edu.cn; melanie.schnell@desy.de; mfzhou@fudan.edu.cn

KEYWORDS: water clusters; microsolvation; noncovalent interaction; microwave spectroscopy; Chirped pulse.

ABSTRACT: The investigation on the preferred arrangement and intermolecular interactions of gas phase solute-water clusters gives insight into the intermolecular potentials that govern the structure and dynamics of the aqueous solutions. Here, we report the investigation of hydrated coordination networks of benzaldehyde-$(water)_n$ (n = 1-6) clusters in a pulsed supersonic expansion using broadband rotational spectroscopy. Benzaldehyde (PhCHO) is the simplest aromatic aldehyde that involves both hydrophilic (CHO) and hydrophobic (phenyl ring) functional groups, which can mimic molecules of biological significance. For the n = 1-3 clusters, the water molecules are connected around the hydrophilic CHO moiety of benzaldehyde through a strong CO···HO hydrogen bond and weak CH···OH hydrogen bond(s). For the larger clusters, the spectra are consistent with the structures in which the water clusters are coordinated on the surface of PhCHO with both the hydrophilic CHO and hydrophobic phenyl ring groups being involved in the bonding interactions. The presence of benzaldehyde does not strongly interfere with the cyclic water tetramer and pentamer, which retain the same structure as in the pure water cluster. The book isomer instead of cage or prism isomers of water hexamer is incorporated into the microsolvated cluster. The PhCHO molecule deviates from the planar structure upon sequential addition of water molecules. The PhCHO-$(H_2O)_{1-6}$ clusters may serve as a simple model system in understanding the solute-water interactions of biologically relevant molecules in aqueous environment.

INTRODUCTION

Water is of fundamental importance for our existence on this planet, and it is involved in nearly all chemical and biological processes.[1] The water-solute interactions and the different ways in which water molecules bind themselves together in highly dynamic and complex networks lie at the heart of solvation chemistry as well as biomolecular folding and assembly. The accurate description of different forms and intermolecular potential of water-solute interactions has been one of the most important subjects in chemistry, which is now receiving increased attention.[1-21]

Water-solute clusters in gas phase serve as simple models in understanding the structures and intermolecular interactions in the bulk water solutions.[1, 20] When incorporating a solute molecule into a water cluster, the intermolecular interactions become more complicated. The energetically preferred structures of large clusters, governed by the subtle interplay of different kinds of noncovalent interactions, are difficult to predict. Their potential energy surface is often characterized by shallow and quasi-degenerate local minima, whose number increases with the dimensions (degrees of freedom) and the size of the clusters. In addition, zero-point energy can play an important role and tip the balance of the energy ordering of different cluster isomers.[22]

From the experimental point of view, spectroscopic techniques such as photoelectron spectroscopy and especially IR action spectroscopy, which has a high efficiency of counting ions, have been applied to study solute-water clusters. However, these techniques often face the dilemma of identifying the detailed structures of neutral clusters.[23-27] Microwave spectroscopy is a powerful tool for precise measurement of geometric structures of weakly bound molecular clusters in the gas phase.[28-31] This technique can routinely achieve frequency resolution better than 10 kHz (10^{-7} cm^{-1}). Therefore, a chemical species, even in complex mixtures,

can be unambiguously resolved and identified.[20] The high spectral resolution of contemporary Fourier transform microwave spectroscopy can fully resolve several closely spaced rotational spectra of isotopically labeled species. By means of Kraitchman's equations, the small differences in the moments of inertia of isotopic species can be used to obtain the substituted atom positions without any structural assumption from theoretical calculations.[32] With the invention of broadband chirped-pulse Fourier transform microwave (CP-FTMW) spectroscopy, it is now possible to collect ~10^6 resolution elements over several GHz in a single signal acquisition event.[33, 34] This fast spectral acquisition over broad frequency ranges rapidly changed the applicability of rotational spectroscopy for the studies of large clusters. It has been successfully employed to determine the stable structures of water clusters including water hexamer,[35, 36] heptamer,[37] nonamer and decamer.[38] These investigations explicitly painted the 3D picture and internal dynamics of water at the onset of aggregation.

Microwave spectroscopy has also been applied to solute-water clusters. Due to the low number density of clusters in the molecular beam, there are very few studies with rotational resolution of solute-$(H_2O)_n$ clusters involving more than four water molecules.[20, 39-43] Regarding hydrated aromatic compound clusters, which are of biological and astronomical importance, up to four water molecules have been reported in the study of acenaphthene-$(H_2O)_{1-4}$.[39]

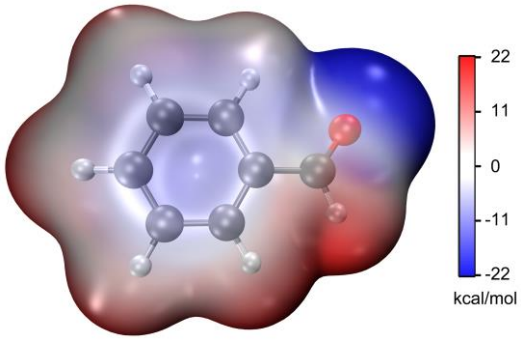

Scheme 1. Electrostatic potential surface of benzaldehyde.

Herein, we report a microwave spectroscopy study on the PhCHO-$(H_2O)_n$ clusters produced in a pulsed supersonic expansion using broadband CP-FTMW spectrometers. The spectra of clusters with n = 1-6 are reported. As the simplest aromatic aldehyde, PhCHO is composed of both hydrophilic (CHO) and hydrophobic (phenyl ring) functional groups (see scheme 1 the electrostatic potential surface of PhCHO), which can mimic molecules of biological significance. The observed water networks in these clusters change from a chain to a cyclic structure, and then to a three-dimensional structure with increasing the number of water molecules. With the number of waters growing, the water binding site extends from the hydrophilic CHO site to the hydrophobic ring site and creates a single water layer covering the solute molecule.

EXPERIMENTAL AND COMPUTATIONAL METHODS

Experimental details: The microwave spectra of benzaldehyde-water clusters were measured using the broadband CP-FTMW spectrometers[44] at DESY (Hamburg) and Fudan university (Shanghai). The diagram of the instrument (Shanghai) is shown in Scheme S1 of Supporting Information. Benzaldehyde was purchased from Sigma-Aldrich (purification > 99.5%) and used without further purification. It was placed in a reservoir, which is custom-made as part of the pulsed valve (General valve series 9), located close to the valve orifice and kept at room temperature. A second reservoir located upstream outside of the vacuum chamber was used for distilled water. Samples with different ratios of $H_2{}^{16}O/H_2{}^{18}O$ (1:0, 3:1, and 0:1) were used. Neon at 3 bars of backing pressure was used as carrier gas. A pulsed supersonic jet (operated at 8 Hz at Hamburg and 9Hz at Shanghai) was generated by the expansion of the gas mixture into the vacuum chamber through a 1 mm diameter nozzle. After a delay of approximately 900 μs, eight back-to-back chirped pulses with a duration of 4 μs spanning the 2-8 GHz frequency range were broadcast into the vacuum chamber through a horn antenna to interact with each molecular beam pulse. The chirped pulses were generated by a 25 GS/s arbitrary waveform generator (AWG) and amplified by a 300 Watts traveling wave tube amplifier (TWTA). The subsequent eight free induction decay (FID) signals of the macroscopic dipole moment of the ensemble of molecules were collected for 40 μs with another horn antenna, amplified, and recorded with a digital oscilloscope in the time domain. The signals were then transformed to the frequency domain by the application of Fourier transformation. A fast-frame data acquisition scheme for eight excitation and emission cycles per supersonic expansion has been used to reduce measurement time and sample consumption. The spectra have an accuracy in the frequency measurement better than 15 kHz and a resolution better than 25 kHz.

Spectral assignment and fitting: The molecular rotational spectrum originates from transitions between the quantized energy levels for molecular rotation. The Hamiltonian operator for rotational kinetic energy is: [28]

$$\boldsymbol{H_{rot} = H_r + H_d}$$

$$\boldsymbol{H_r = AP_a^2 + BP_b^2 + CP_c^2}$$

In these expressions, H_r is the rigid rotor term, H_d is the centrifugal distortion term, P_a, P_b, and P_c are the angular momentum operators for rotational motion about the three principal axes of rotation, and A, B, and C are the rotational constants. The rotational constants are inversely related to the principal moments-of-inertia that characterize the three-dimensional mass distribution of the molecule. The interaction of the microwave source with the dipole moment changes the rotational kinetic energy around the three principal axes, which results in three types of rotational spectra, known as *a*-type, *b*-type, and *c*-type. The relative intensities of these spectra are proportional to the square of the respective dipole moment component. The experimental rotational constants combined with the dipole moments can provide structural information for the assigned molecules.

Initial spectral assignments of the rotational transitions were obtained using the JB95 program.[45] Refined fits were achieved using the AABS suite[46] with a standard Watson-type Hamiltonian (*S*-reduction and I^r representation)[47] as implemented in Pickett's SPFIT.[48]

The positions of individual atoms in the principal axis system can be determined by rotational spectroscopy with isotopic substitutions without any calculated assumption of initial structures.[32] The approach is based on the Born-Oppenheimer approximation that the atom positions in the molecular structure are isotope independent. With a single isotopic substitution for each different atom, the mass distribution will change. By measuring the changes in the rotational constants upon single isotopic substitution, the changes in the three moments-of-inertia can be converted to the atom coordinates in the principal axis system (r_s). In an alternative way, starting with an initial structure, which is generally obtained from quantum chemical calculations, the moments-of-inertia can be changed by adjusting some structural parameters. In a least-squares fitting procedure, the experimental moments-of-inertia can be reproduced, and the fitted structure can be obtained, which is regarded as the effective structure of the ground state (r_0). In the cases where vibrational–rotational effects occur, additional parameters are added to the fit, and the mass-dependent molecular structure, which is close to the experimental equilibrium structure, $r_m^{(1)}$, is obtained.[28, 49, 50]

Quantum chemical calculations: The conformational search of benzaldehyde-water clusters was performed using the CREST/GFN-xTB software.[51] The energetically low-lying structures with a 20 kJ/mol energy threshold were then reoptimized at the B3LYP-D4/def2-TZVP level of theory[52] using the Orca package.[53] Harmonic frequency calculations were performed at the same level to confirm the real potential minima and to obtain their zero-point vibrational energies (ZPVE). The basis set superposition error (BSSE) was also considered for the binding energies of the clusters. To visualize the intermolecular interactions, we used the noncovalent interaction (NCI) approach, which is based on the electron density and its derivatives.[54] The intuitive description indicates where the strong hydrogen bonds and weak attractive interactions occur. The analysis for NCI was generated with the Multiwfn software,[55] and the plots were carried out with the Chimera software.[56] The lowest-energy complexes optimized at the B3LYP-D4/def2-TZVP level of theory were used as inputs for these analyses.

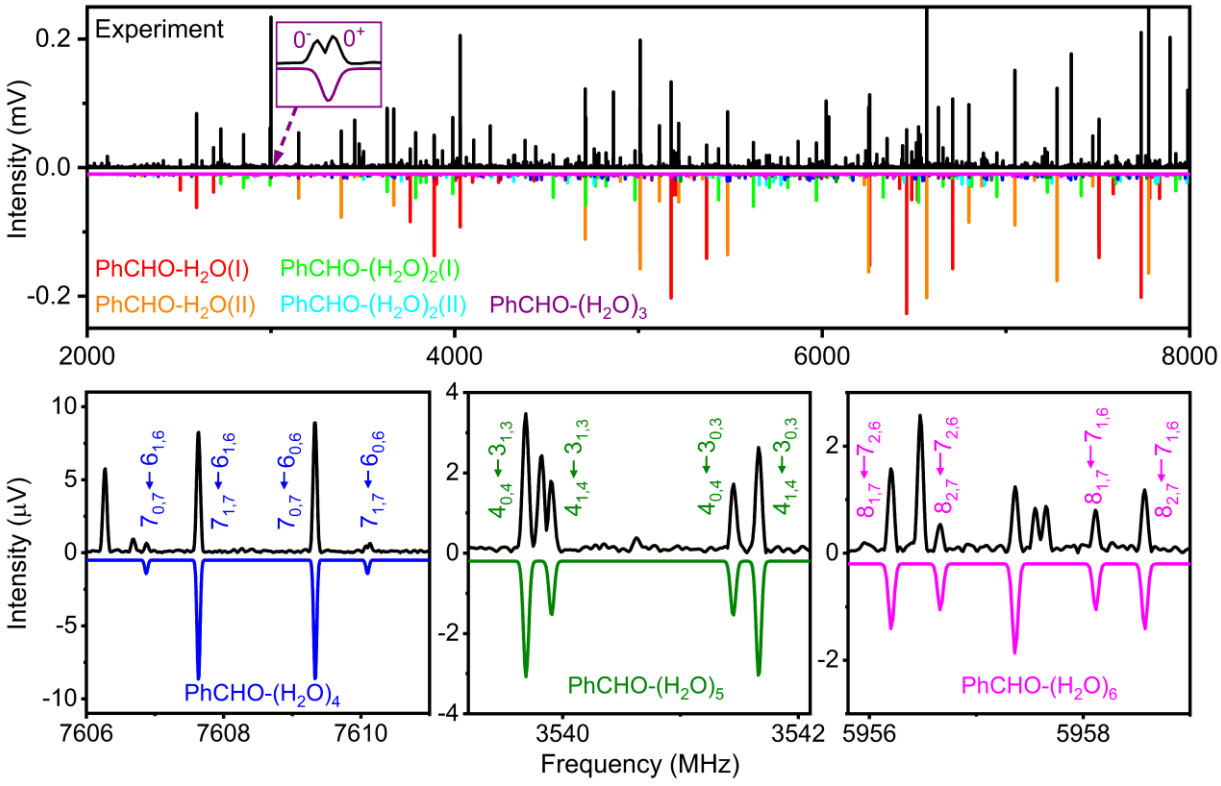

Figure 1. Broadband rotational spectra of PhCHO-$(H_2O)_{1\text{-}6}$. The black upper trace corresponds to the experimental spectrum after removing the spectral lines arising from the PhCHO monomer (9.5 million FID average). The lower traces in different colors represent simulated spectra of PhCHO-$(H_2O)_{1\text{-}3}$ from the experimental spectroscopic parameters (Tables 1 and 2), at a rotational temperature of 1 K, and the theoretical dipole moment components for the respective complexes. The inset highlights the tunnelling splitting of PhCHO-$(H_2O)_3$. At the bottom, parts of the spectra highlight representative transitions from the n = 4-6 clusters. The quantum numbers are defined using the standard nomenclature for the rotational energy levels of an asymmetric top, denoted as $J_{Ka,Kc}$, where J is the quantum number for the total rotational angular momentum, and K_a and K_c are the quantum numbers for the projection of the total rotational angular momentum onto the rotational axes (a and c) in the two limiting cases of prolate and oblate symmetric tops, respectively.

RESULTS AND DISCUSSION

The rotational spectra were measured within the frequency range covering 2 to 8 GHz using different water samples that contain pure $H_2{}^{16}O$, pure $H_2{}^{18}O$, and a mixture of $H_2{}^{16}O$ and $H_2{}^{18}O$ with a 3:1 ratio, respectively. As expected, the rotational spectra of the PhCHO molecule and the water dimer $(H_2O)_2$ are the most intense contributors. The spectra of PhCHO monomer in the 6-41 and 170-330 GHz ranges have been reported in a previous work.[57] In our spectrum, interestingly, the signal intensity of the species containing the ^{18}O labeled carbonyl group is much stronger in the experiment with the $H_2{}^{18}O$ sample. This is due to oxygen-atom exchange between the -CHO group and H_2O, a process similar to the one that has been observed in the study of the rotational spectroscopy of acrolein-water complexes.[58] The spectroscopic parameters of different isotopologues of the PhCHO monomer determined from the spectrum in the 2-8 GHz range are listed in Table S1. The substitution coordinates (r_s) from Kraitchman's equations and the fitted structural parameters (r_s, and $r_m^{(1)}$) are listed in Tables S2 and S3. These data are in agreement with those reported previously derived from the high frequency spectral range.[57] The equilibrium coordinates and structural parameters predicted at the B3LYP-D4/def2-TZVP level of theory are also listed in Tables S2 and S3 for comparison. The results show good agreement between experiments and quantum chemical calculations.

Figure 1 shows the experimental spectrum after removing the spectral lines arising from the PhCHO monomer. The most intense rotational transitions in Figure 1 are assigned to two PhCHO-H_2O conformational isomers (see Figure 1). Guided by the prediction from theoretical calculations, two groups of rotational transitions can be straightforwardly assigned to two PhCHO-$(H_2O)_2$ isomers with the rotational constants being listed in Table 1. The small values of the planar moments of inertia along the *c* principal axis (P_{cc}) imply that these vibrationally averaged structures are planar (see Table 1). Due to the high signal-to-noise ratio of the spectra for these clusters, we can also assign the rotational transitions of their singly ^{13}C-substituted isotopologues. The next group of *a*-type transitions could be assigned to the PhCHO-$(H_2O)_3$ cluster, among which some of the transitions split into two closely spaced components (see the inset of Figure 1). The spectral splitting is the result from a large-amplitude motion along a symmetric potential, which usually can lift the degeneracies of the vibrational levels in this symmetric potential (vide infra).[59]

Besides the spectral lines of the PhCHO-$(H_2O)_n$ (n=1-3) clusters, abundant but low intensity spectral lines are present in the spectrum. Among these lines, some interesting spectral patterns can clearly be identified, which are quartets with two pairs of equally spaced spectral lines. Some representative transitions are shown in the bottom panel of Figure 1. These spectral features are consistent with the transitions of systems consisting of four quantum energy levels, in which two of them are *a*-type transitions while the other two are *b*-type transitions, or they are *b*-type combined with *c*-type transitions. Following this general hint, we initially fit these frequencies to three independent rotational Hamiltonians and succeeded to include more rotational transitions over the course of the analysis. By comparing the fitted spectroscopic parameters with those derived from high-level quantum chemical calculations, the spectra are assigned to the PhCHO-$(H_2O)_4$, PhCHO-$(H_2O)_5$, and PhCHO-$(H_2O)_6$ clusters, respectively, as listed in Table 2. In the $H_2{}^{18}O$-containing broadband spectra, we can assign the ^{18}O-enriched species for the PhCHO-$(H_2O)_{1\text{-}3}$ clusters; however, we were not able to assign any for the larger clusters. This finding is understandable because the diluted populations of different isotopologues in the molecular beam significantly decreased their signal intensity from that of their already weak parent species. In addition, the oxygen-atom exchange between PhCHO and water makes the situation more complicated as well. The experimentally observed frequencies and their assignments are listed in Tables S26-S34, respectively.

For the PhCHO-$(H_2O)_{1\text{-}2}$ clusters, the structural parameters (r_s, r_0/r_m) of the heavy atom frameworks are derived from their isotopic rotational constants. For PhCHO-$(H_2O)_3$, the positions of the oxygen atoms in the water molecules can be experimentally determined from the ^{18}O enriched spectra. These data are listed in Tables S5, S6, S8, S9, S12, S13, S15, S16, S18, S19.

Quantum chemical calculations were performed for the PhCHO-$(H_2O)_n$ (n=1-6) clusters. The low-lying stable conformers for each cluster calculated at the B3LYP-D4/def2-TZVP level of theory are listed in Tables S35-S40. The most stable conformers of the n=1-3 clusters are shown in Figure 2. The optimized hydrogen bonding parameters (C···O and O···O distances) together with the experimentally fitted values are listed. The NCI plots mapping the location and strength of the noncovalent interactions are also shown in Figures 2 and 3. A hydrogen bond OH···$O_{carbonyl}$ between a water molecule and the carbonyl group of PhCHO is present in all the clusters.

Table 1. Comparison between the experimental and simulated spectroscopic parameters of the PhCHO-$(H_2O)_{1,2}$ clusters.

	PhCHO-H_2O_(I)		PhCHO-H_2O_(II)		PhCHO-$(H_2O)_2$_(I)		PhCHO-$(H_2O)_2$_(II)	
	Expl.	Calc.	Expl.	Calc.	Expl.	Calc.	Expl.	Calc.
A[MHz]	4609.3877(27)[a]	4691.5[b]	2732.5980(17)	2755.8	2504.9934(12)	2586.3	1497.61477(68)	1558.6
B[MHz]	694.37090(50)	697.4	981.80018(77)	1013.2	521.84825(22)	525.8	797.12914(46)	789.8
C[MHz]	603.86222(47)	607.4	722.99239(72)	741.4	432.45243(21)	438.2	521.33059(27)	528.9

D_J[kHz]	0.1293(86)		0.269(16)		0.0971(14)		0.3339(58)	
D_{JK}[kHz]	-1.762(33)		-0.413(62)		-0.7224(66)		-1.159(26)	
d_1[kHz]			-0.0835(41)		-0.0255(13)		-0.1386(34)	
$\mu_a/\mu_b/\mu_c$	Y/Y/N[c]	3.7/0.1/0.7	Y/Y/N	2.9/1.0/0.7	Y/Y/N	2.9/0.1/0.1	Y/Y/N	2.9/1.0/0.2
P_{cc}[μÅ²]	0.27649(42)		0.34085(41)		0.77714(35)		1.02634(32)	
σ[d][kHz]	7.860		8.753		3.886		3.859	
N[e]	45		45		64		45	

[a] Standard errors within parentheses are expressed in units of the last two digits. [b] calculated at B3LYP-D4/def2-TZVP level of theory. [c] Y/N denotes that the corresponding transitions were observed/not observed. [d] Root-mean-square deviation of the fit. [e] number of the lines in the fit.

Table 2. Comparison between the experimental and simulated spectroscopic parameters of the PhCHO-$(H_2O)_{3-6}$ clusters.

	PhCHO-$(H_2O)_3$		PhCHO-$(H_2O)_4$		PhCHO-$(H_2O)_5$		PhCHO-$(H_2O)_6$	
	Expl.	Calc.	Expl.	Calc.	Expl.	Calc.	Expl.	Calc.
A[MHz]	1438.7861(69)[a]	1508.7[b]	844.63511(66)	874.8	610.05086(37)	620.9	530.48882(40)	523.6
B[MHz]	454.65050(81)	455.7	646.24247(40)	661.6	559.16530(54)	588.0	442.34902(28)	479.2
C[MHz]	351.25839(64)	354.7	529.76060(31)	544.2	422.56078(33)	438.4	347.58346(19)	344.3
D_J[kHz]	0.0979(24)		0.2232(39)		0.1130(33)		0.1452(22)	
D_{JK}[kHz]	-0.454(29)		-0.480(15)				-0.467(11)	
D_K[kHz]			0.707(37)				0.693(10)	
d_1[kHz]	-0.0233(25)		-0.0601(26)		-0.0221(20)		-0.0445(11)	
$\mu_a/\mu_b/\mu_c$	Y/Y/N[c]	1.3/0.1/0.7	Y/Y/Y	3.1/0.8/1.3	Y/Y/Y	0.8/2.5/0.7	Y/Y/Y	2.0/2.2/0.8
P_{cc}[μÅ²]	12.0318(19)		213.19538(44)		268.11975(69)		320.58852(65)	
σ[d][kHz]	9.028		5.256		9.718		8.405	
N[e]	49		71		98		157	

[a] Standard errors within parentheses are expressed in units of the last two digits. [b] calculated at B3LYP-D4/def2-TZVP level of theory. [c] Y/N denotes that the corresponding transitions were observed/not observed. [d] Root-mean-square deviation of the fit. [e] number of the lines in the fit.

For the n = 1 complex, there are two close-lying isomers associated with the structures in which the water molecule is located at either side of the carbonyl group within the PhCHO molecule plane. The first structure (Figure 2a) involves a secondary weak CH···O hydrogen bond between the hydrogen atom of the aldehyde group and the oxygen atom of water, while the second structure contains a secondary weak CH···O hydrogen bond between the hydrogen atom of the phenyl ring and the water oxygen atom (Figure 2b). The first structure is predicted to be 2.9 kJ/mol less stable than the second structure after zero-point energy and basis set superposition error corrections. The calculated hydrogen bonding C···O and O···O distances are slightly shorter than the experimental values (Figure 2). As listed in Table 1, the calculated rotational constants (A, B, C) are in excellent agreement with the experimental values for both isomers.

For the n = 2 cluster, two close-lying structural isomers have been assigned. In the first isomer (Figure 2c), the two water molecules form an OH···O hydrogen bond and coordinate with the aldehyde group via an OH···$O_{carbonyl}$ hydrogen bond and a CH···O hydrogen bond forming a cyclic structure. In the second isomer, only the O atom of the aldehyde group is involved in forming an OH···$O_{carbonyl}$ hydrogen bond with one water molecule. Besides the strong OH···O hydrogen bond, the two water molecules form weak CH···O hydrogen bonds with the hydrogen atoms of the phenyl ring (Figure

2d). The first structure involves a stronger hydrogen bond between the water molecules with a shorter O···O distance. The first structure is predicted to be 1.5 kJ/mol more stable than the second structure at the B3LYP-D4/def2-TZVP level. The calculated rotational constants match the experimental values very well (Table 1) and support the experimental assignment.

For the n = 3 cluster, the experimentally observed structure can be attributed to the predicted most stable structure (Figure 2e). In this structure, the three water molecules form a chain instead of the cyclic structure of the isolated water trimer observed in the gas phase.[60] The hydrogen-bonding fashion is similar to those in the n = 1 and 2 complexes. The O-O-O water chain has an experimentally determined angle of 112.0(1)°. It interacts with PhCHO and binds to the carbonyl oxygen atom on one end and to two hydrogen atoms in a bifurcated manner on the other end. The middle water molecule is squeezed out of the plane defined by the PhCHO molecule, and forms a weak CH···O hydrogen bond with the hydrogen atom of the aldehyde group (Figure 2e). This structural characteristic coincides with the increased planar moment of inertia (P_{cc}=12.0318, see Table 2) with respect to those of the n=1, 2 clusters. This structure can undergo a puckering motion with the middle water molecule moving above and below the symmetric plane. This is similar to the motion observed in the pure water pentamer and indan.[61,62] This puckering motion is responsible for the observed splitting of the rotational transition of PhCHO-$(H_2O)_3$. The barrier for this puckering motion is predicted to be 9.2 kJ mol^{-1} at the B3LYP-D4/def2-TZVP level. The oxygen atom of the middle water has to move 2.02 Å going from the puckered-up to the puckered-down structure. The next structure is predicted to be 1.5 kJ/mol higher in energy than the most stable isomer. It has a similar water arrangement and rotational constants as the most stable structure but differs for the free OH bond orientations.

For the larger PhCHO-$(H_2O)_{4-6}$ clusters, a set of structures in which PhCHO is attached to different binding sites of a known water cluster structure is considered. The preferred results based on molecular force field and semiempirical searches have also been considered and further optimized with high-level quantum chemical calculations. As listed in Tables S38-S40, a total of 20, 58 and 35 isomers within a 10 kJ/mol relative energy window have been found for the n=4, 5 and 6 clusters, respectively. The most stable isomers of the PhCHO-$(H_2O)_{4-6}$ clusters are shown in Figure 3 (and Figures S7, S10, S13, and S16). For each cluster, the calculations give two nearly isoenergetic isomers, which differ only in the clockwise or anticlockwise orientations of the endocyclic hydrogen bonds of the water cluster. The two isomers have essentially the same rotational constants and dipole moment components since they only differ in the sense of rotation of the hydrogen-bond network. The calculated rotational constants for both isomers are similar to the experimental values (Figure S16); thus, we cannot unambiguously identify which isomer is experimentally observed. Here we only give an inconclusive structural preference depending on the predicted relative energy. The conformation with an anticlockwise cyclic hydrogen bonded water arrangement is slightly lower in energy than the clockwise cyclic one for the n = 4 and 6 clusters, while the clockwise cyclic conformer is 0.1 kJ/mol lower than the other for the n = 5 cluster. For each cluster, the other low-lying conformer would also be present in the supersonic expansion, but as the transition intensities of the identified species are already weak, it is plausible to expect that it would be difficult to identify them (see Figure S18).

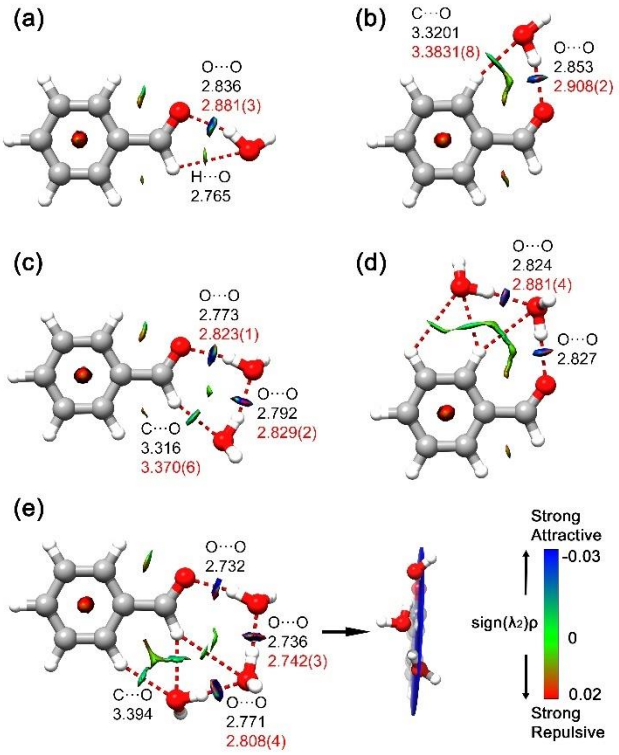

Figure 2. The optimized hydrogen bonding parameters r_e (black) at the B3LYP-D4/def2-TZVP level of theory, compared with the experimental values r_s (red) of the PhCHO-$(H_2O)_{1-3}$ clusters. All distances are in Å. (a) PhCHO-H_2O_(I), (b) PhCHO-H_2O_(II), (c) PhCHO-$(H_2O)_2$_(I), (d) PhCHO-$(H_2O)_2$_(II), and (e) PhCHO-$(H_2O)_3$, with a side view shown on the right side. The NCI plots (reduced density gradient) mapping the location and strength of noncovalent interactions are also shown. The gradient isosurfaces (s = 0.5 a.u.) are colored on a blue-green-red scale according to values of the electron density multiplied by the sign of the second Hessian eigenvalue (sign(λ_2)ρ), ranging from -0.03 to 0.02 a.u. Blue indicates strong attractive interaction, green indicates weak attractive interaction, and red indicates strong repulsive interaction.

The bonding layout of these larger clusters undergoes a drastic change compared to those of the smaller clusters. The water molecules do not bind sideways to the PhCHO molecule as previously seen, but they are located on top of the molecular plane of the phenyl ring. As shown in Figure 3, the arrangement of the water molecules in the n=4 cluster is quite similar to that of the pure water tetramer.[63] The four water molecules form a cyclic hydrogen-bonded structure in which each water molecule contributes one OH moiety to form a hydrogen-bonded water tetramer ring. The

remaining hydrogen atoms point out of the plane defined by the water ring in an up-down-up-down orientation leaving two free hydrogen atoms. One down-orientated hydrogen atom is bound to the oxygen atom of the carbonyl group forming an OH···O hydrogen bond, while the other down-orientated hydrogen atom points to the phenyl ring and forms an OH···π interaction. Therefore, both the hydrophilic (CHO) and hydrophobic (phenyl ring) sites of PhCHO are connected with water through a hydrogen bonding network. As a comparison, the vibrational spectroscopy of phenol-$(H_2O)_n$ clusters has indicated that only the hydrophilic group is involved in the water network.[64-66] A similar result has also been reported in the rotational spectroscopic study of hydrated glycolaldehyde clusters, where only the oxygen atom and the hydroxyl group of glycolaldehyde form hydrogen bonds with water molecules.[67]

A similar hydrogen bonding architecture can be found in the PhCHO-$(H_2O)_5$ cluster. A cyclic water pentamer similar to the structure of the pure water pentamer lies on top of the PhCHO plane.[61] The orientations of the five free hydrogen atoms appear as an up-up-down-up-down arrangement. As in the PhCHO-$(H_2O)_4$ cluster, the two down-orientated hydrogen atoms interact with PhCHO via an OH···$O_{carbonyl}$ bond and an OH···π bond.

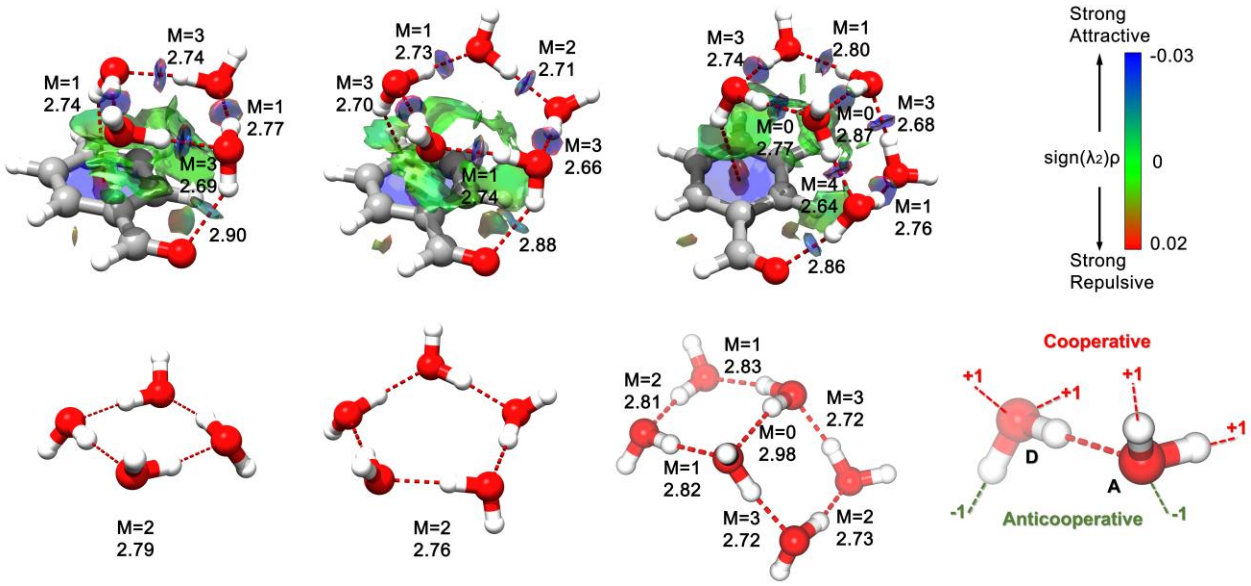

Figure 3. The oxygen–oxygen distances (Å) and the net hydrogen bond cooperativity (M) in the PhCHO-$(H_2O)_{4-6}$ and pure water clusters $(H_2O)_{4-6}$. The net cooperativity of a donor–acceptor (D–A) hydrogen bond is determined by calculating the sum of all cooperative neighboring hydrogen bonds (+1) and anticooperative hydrogen bonds (−1), as shown in the bottom-right diagram. The NCI plots mapping the location and strength of noncovalent interactions in the PhCHO-$(H_2O)_{4-6}$ clusters are also shown. The gradient isosurfaces (s = 0.5 a.u.) are colored on a blue-green-red scale according to values of the electron density multiplied by the sign of the second Hessian eigenvalue (sign(λ_2)ρ), ranging from -0.03 to 0.02 a.u. Blue indicates strong attractive interaction, green indicates weak attractive interaction, and red indicates strong repulsive interaction.

The water hexamer is the smallest sized water cluster to exhibit a three-dimensional hydrogen bonding network, existing as several competing structures, including cage, prism, book, bag, and cyclic forms.[35, 36, 64, 68-70] Cristóbal Pérez and co-workers established the population ratio for the three lowest energy isomers cage, prism, and book to be 1 : 1 : 0.25 in a supersonic beam with neon and helium as carrier gas, while only the cage isomer was observed using argon as carrier gas.[35] Similar to the pure water hexamer, several isomers similar in energy were found by theoretical calculations for PhCHO-$(H_2O)_6$ (Figure S13 and Table S40). All of the calculations suggest that the book-incorporated structure is energetically preferred. The rotational constants of the book-incorporated structure are in good agreement with the experimental results (see Table 2 and Figure S16). No isomers involving cage and prism structures of the $(H_2O)_6$ moiety were assigned, even though the previous microwave spectroscopic study has shown that the cage and prism isomers are more stable than the book isomer for the pure water hexamer.[35] The calculated rotational constants of these low-lying isomers do not fit the experimental values. The result indicates that the relative stability of the water hexamer isomers is altered by coordination with a planar aromatic molecule, but the transition from cyclic to three-dimensional structures of water clusters still occurs at n = 6 in the PhCHO-$(H_2O)_n$ clusters. This observation is similar to the results of an infrared spectroscopic study of benzene-$(H_2O)_6$, in which the single observed isomer of benzene-$(H_2O)_6$ incorporates an inverted book structure rather than the cage or prism.[25]

The free PhCHO molecule is planar due to the π-π conjugation. Upon coordination by the water clusters, the PhCHO molecule becomes nonplanar. The variation of the dihedral angle between the phenyl ring and the aldehyde group as a function of the number of water molecules is shown in Figure 4. The PhCHO molecule differs only slightly from the planar structure upon coordination with up to five water

molecules. The dihedral angle drastically increases when the hydrated cluster grows to PhCHO-$(H_2O)_6$, which shows the solvation effect of 3D structured water hexamer.

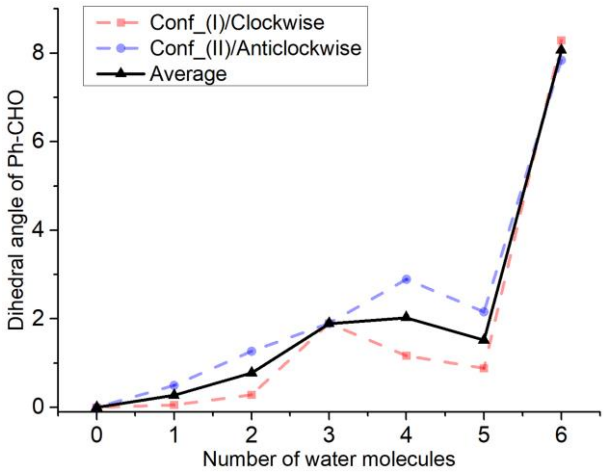

Figure 4. The variation of dihedral angle of Ph-CHO (in degrees) as a function of the number of water molecules in the PhCHO-$(H_2O)_n$ clusters. The red dashed line represents the conformer_(I) of PhCHO-$(H_2O)_{1\text{-}2}$ and clockwise conformations of PhCHO-$(H_2O)_{4\text{-}6}$, while the blue line is the conformer_(II) and anticlockwise conformations. The black trace is the average for each cluster.

The binding energies between benzaldehyde and water clusters in the PhCHO-$(H_2O)_n$(n=1-6) clusters calculated at the B3LYP-D4/def2-TZVP level after ZPVE and BSSE corrections are listed in Table S41. The binding energy increases from n=1 to n=2 and 3 due to increased binding sites between PhCHO and water. However, the binding energy decreases from n=3 to n=4. The binding energy increases with increasing cluster size from n=4 to 6. The number of binding sites between PhCHO and water (OH···$O_{carbonyl}$ and OH···π) no longer increases in the larger clusters. The increase in binding energy is largely due to increased dispersion interaction as shown in Table S42.

The PhCHO-water interactions strengthen the hydrogen bonding networks of the water clusters in the larger PhCHO-$(H_2O)_n$ (n=4-6) clusters, and this results in the slightly distorted cyclic and book structures of water clusters. These structural manifestations can be explained by net cooperativity effects.[38, 39] Net cooperativity effects are defined as parameter *M*, which accounts for the potential two-body and three-body hydrogen bonds of the donor (D)–acceptor (A) pairs. The values of *M* can range from −2 to 4, with larger numbers indicating a stronger hydrogen bond and a shorter donor–acceptor distance. Net cooperativity effects are governed by the local environment of a water molecule. This environment changes as the potential for the water molecule to form hydrogen bonds increases or decreases. The results from this analysis are reported in Figure 3 and S19, where we compare the net cooperativity values for each hydrogen bond in the PhCHO-$(H_2O)_{4\text{-}6}$ with those in the bare water cluster. We observe that upon complexation, the *M* values, and therefore the strength of the hydrogen bond, is increased as two new bonds are established. This is nicely captured by our cooperativity analysis as the larger M values correspond to the shortest O···O distances. In particular, the formation of an OH···π bond is likely responsible for the transition from an in-plane cluster growth for PhCHO-$(H_2O)_{1\text{-}3}$ to an above-plane arrangement observed in the larger clusters. These interactions offer an additional anchoring site that shapes the structure of the cluster while keeping the main OH···$O_{carbonyl}$ bond. They are illustrated in Figure 3 as a green, delocalized isosurface that involves the phenyl ring. As shown, although these interactions lower the M value of one bond, it simultaneously increases the strength of the immediately adjacent hydrogen bond. Overall, the energetic balance is favorable thanks to the new interaction and cooperative effects are apparent with a clear shortening of the hydrogen bond with respect to those in the bare water cluster. For clusters ranging from one to three water molecules, this interaction is not possible without largely impacting the dominant OH···$O_{carbonyl}$ hydrogen bond due to geometrical restrictions. This sets a transition point to above-plane cluster growth, when the dimension of the hydrogen bond network is large enough to favorably reach the ring π cloud while unaffecting the OH···$O_{carbonyl}$ interaction. These results highlight how the molecular shape can drastically change as the size of the cluster grows as new interactions are established.

CONCLUSIONS

The rotational spectra of the PhCHO-$(H_2O)_n$ clusters generated in a supersonic expansion molecular beam are measured in the 2-8 GHz spectral range using broadband chirped-pulse Fourier transform microwave spectrometers. The rotational spectra of the n=1-6 clusters are assigned, and the structures of the topology of the clusters has been unambiguously determined, which are also predicted to be the most stable structures by quantum chemical calculations. The results clearly show the transformations of the hydrated coordination network from chain-like to cyclic and then to 3D arrangement with the sequential addition of water molecules. For the n = 1-3 clusters, the structures of heavy atom frameworks determined via isotopically substituted spectra indicate that the water molecules are connected sideways around the hydrophilic CHO moiety of benzaldehyde through a strong CO···HO hydrogen bond and weak CH···OH hydrogen bond(s). For the n = 4 and 5 clusters, the spectra are consistent with the structures in which the cyclic water clusters are coordinated on the surface of the benzaldehyde molecular plane. The spectrum of the n = 6 cluster has been assigned to a cluster incorporating an inverted book isomer of water hexamer that resembles a single water layer mantling the surface of benzaldehyde. PhCHO is the simplest aromatic aldehyde that involves both hydrophilic (CHO) and hydrophobic (phenyl ring) functional groups which can mimic molecules of biological significance. The PhCHO-$(H_2O)_{1\text{-}6}$ clusters may serve as simple model system in understanding the solute-water interactions of biologically relevant molecules in aqueous environment.

ASSOCIATED CONTENT

Supporting Information.

Experimental spectroscopic parameters of the isotopologues of PhCHO-$(H_2O)_n$, n=0-6;
Equilibrium coordinates (r_e) calculated at the B3LYP-D4/def2-TZVP level of theory and substitution coordinates (r_s) from Kraitchman's equations for single isotopic substitution;
r_e (at the B3LYP-D4/def2-TZVP level of theory), r_s, $r_m^{(1)}$, and r_0 structural parameters;
Experimental transition frequencies (ν/MHz) together with the corresponding observed - calculated differences ($\Delta\nu$/kHz) for each species;
Relative energies (in kJ/mol), rotational constants (in MHz), dipole moment components (in Debye) of the stable conformers of each clusters searched using the CREST/GFN-xTB software and then optimized at the B3LYP-D4/def2-TZVP level of theory.
These materials are available free of charge via the Internet at http://pubs.acs.org.

AUTHOR INFORMATION

Corresponding Authors

Weixing Li - Department of Chemistry, Shanghai Key Laboratory of Molecular Catalysis and Innovative Materials, Fudan University, Songhu Rd. 2005, 200438 Shanghai, China; orcid.org/0000-0003-0169-0990; Email: weixingli@fudan.edu.cn
Melanie Schnell - Deutsches Elektronen-Synchrotron DESY, Notkestraße 85, 22607 Hamburg, Germany; Christian-Albrechts-Universität zu Kiel, Institute of Physical Chemistry, Max-Eyth-Str. 1, 24118 Kiel, Germany; orcid.org/0000-0001-7801-7134; Email: melanie.schnell@desy.de
Mingfei Zhou - Department of Chemistry, Shanghai Key Laborato-ry of Molecular Catalysis and Innovative Materials, Fudan University, Songhu Rd. 2005, 200438 Shanghai, China; orcid.org/0000-0002-1915-6203; Email: mfzhou@fudan.edu.cn

Authors

Cristóbal Pérez - Deutsches Elektronen-Synchrotron DESY, Notkestraße 85, 22607 Hamburg, Germany; Present Address: Departamento de Química Física y Química Inorgánica, Facultad de Ciencias-I.U. CINQUIMA, Universidad de Valladolid, E-47011 Valladolid, Spain; orcid.org/0000-0001-5248-5212
Amanda L. Steber - Deutsches Elektronen-Synchrotron DESY, Notkestraße 85, 22607 Hamburg, Germany; Present Address: Departamento de Química Física y Química Inorgánica, Facultad de Ciencias-I.U. CINQUIMA, Universidad de Valladolid, E-47011 Valladolid, Spain; orcid.org/0000-0002-8203-2174
Dingding Lv - Department of Chemistry, Shanghai Key Laboratory of Molecular Catalysis and Innovative Materials, Fudan University, Songhu Rd. 2005, 200438 Shanghai, China.
Guanjun Wang - Department of Chemistry, Shanghai Key Laboratory of Molecular Catalysis and Innovative Materials, Fudan University, Songhu Rd. 2005, 200438 Shanghai, China; orcid.org/0000-0002-3265-7192
Xiaoqing Zeng - Department of Chemistry, Shanghai Key Laboratory of Molecular Catalysis and Innovative Materials, Fudan University, Songhu Rd. 2005, 200438 Shanghai, China; orcid.org/0000-0003-4611-2094

Author Contributions

The manuscript was written through contributions of all authors. All authors have given approval to the final version of the manuscript.

Funding Sources

This work was financially supported by the National Natural Science Foundation of China (Grants 22103015), and Deutsche Forschungsgemeinschaft (SCHN1280/4-2, project number 271359857) in the context of the priority program SPP 1807 "Control of London dispersion interactions in molecular chemistry".

Notes

The authors declare no conflict of interest.

ACKNOWLEDGMENT

W. Li thanks Jens-Uwe Grabow, Luca Evangelisti, and the FS-SMP group for helpful discussions during the construction of the CP-FTMW spectrometer at Fudan University. We also acknowledge the scientific exchange and support of the Center for Molecular Water Science (CMWS).

REFERENCES

(1) Ludwig, R. Water: From clusters to the bulk. *Angew. Chem. Int. Ed.* **2001**, *40*, 1808-1827.
(2) Liu, K.; Cruzan, J. D.; Saykally, R. J. Water clusters. *Science* **1996**, *271*, 929-933.
(3) Wernet, P.; Nordlund, D.; Bergmann, U.; Cavalleri, M.; Odelius, M.; Ogasawara, H.; Naslund, L. A.; Hirsch, T. K.; Ojamae, L.; Glatzel, P.; Pettersson, L. G. M.; Nilsson, A. The structure of the first coordination shell in liquid water. *Science* **2004**, *304*, 995-999.
(4) Wang, X.; Yang, X.; Nicholas, J. B.; Wang L. Bulk-like features in the photoemission spectra of hydrated doubly charged anion clusters. *Science* **2001**, *294*, 1322-1325.
(5) Mitsui, T., Rose, M. K.; Fomin, E.; Ogletree, D. F.; Salmeron, M. Water diffusion and clustering on Pd(111). *Science* **2002**, *297*, 1850-1852.
(6) Robertson, W. H.; Diken, E. G.; Price, E. A.; Shin, J.; Johnson, M. A. Spectroscopic determination of the OH− solvation shell in the $OH^-\cdot(H_2O)_n$ clusters. *Science* **2003**, *299*, 1367-1372.
(7) Miyazaki, M.; Fujii, A.; Ebata, T.; Mikami, N. Infrared spectroscopic evidence for protonated water clusters forming nanoscale cages. *Science* **2004**, *304*, 1134-1137.
(8) Headrick, J. M.; Diken, E. G.; Walters, R. S.; Hammer, N. I.; Christie, R. A.; Cui, J.; Myshakin, E. M.; Duncan, M. A.; Johnson, M. A.; Jordan. K. D. Spectral signatures of hydrated proton vibrations in water clusters. *Science* **2005**, *308*, 1765-1769.
(9) Turi, L.; Sheu, W.; Rossky, P. J. Characterization of excess electrons in water-cluster anions by quantum simulations. *Science* **2005**, *309*, 914-917.
(10) Verlet, J. R. R.; Bragg, A. E.; Kammrath, A.; Cheshnovsky, O.; Neumark, D. M. Observation of large water-cluster anions with surface-bound excess electrons. *Science* **2005**, *307*, 93-96.
(11) Suma, K.; Sumiyoshi, Y.; Endo, Y.; The rotational spectrum of the water-hydroperoxy radical (H_2O-HO_2) complex. *Science* **2006**, *311*, 1278-1281.
(12) Gutberlet, A.; Schwaab, G.; Birer, Ö.; Masia, M.; Kaczmarek, A.; Forbert, H.; Havenith, M.; Marx, D. Aggregation-induced dissociation of $HCl(H_2O)_4$ below 1 K: The smallest droplet of acid. *Science* **2009**, *324*, 1545-1548.
(13) Relph, R. A.; Guasco, T. L.; Elliott, B. M.; Kamrath, M. Z.; McCoy, A. B.; Steele, R. P.; Schofield, D. P.; Jordan, K. D.; Viggiano, A. A.; Ferguson, E. E.; Johnson, M. A. How the shape of an H-bonded network controls proton-coupled water activation in HONO formation. *Science* **2010**, *327*, 308-312.
(14) Ball, P. Water as an active constituent in cell biology. *Chem. Rev.* **2008**, *108*, 74-108.

(15) Fournier, J. A.; Johnson, C. J.; Wolke, C. T.; Weddle, G. H.; Wolk, A. B.; Johnson, M. A. Vibrational spectral signature of the proton defect in the three-dimensional $H^+(H_2O)_{21}$ cluster. *Science* **2014**, *344*, 1009-1012.

(16) de Tudela, R. P.; Marx, D. Acid dissociation in HCl-water clusters is temperature dependent and cannot be detected based on dipole moments. *Phys. Rev. Lett.* **2017**, *119*, 223001.

(17) Mani, D.; de Tudela, R. P.; Schwan, R.; Pal, N.; Körning, S.; Forbert, H.; Redlich B.; van der Meer, A. F. G.; Schwaab, G.; Marx, D.; Havenith, M. Acid solvation versus dissociation at "stardust conditions": Reaction sequence matters. *Sci. Adv.* **2019**, *5*, eaav8179.

(18) Yang, N.; Duong, C. H.; Kelleher, P. J.; McCoy, A. B.; Johnson. M. A. Deconstructing water's diffuse OH stretching vibrational spectrum with cold clusters. *Science* **2019**, *364*, 275-278.

(19) Tian, Y.; Hong, J.; Cao, D.; You, S.; Song, Y.; Cheng, B.; Wang Z.; Guan, D.; Liu, X.; Zhao, Z.; Li, X.; Xu, L.; Guo, J.; Chen, J.; Wang, E.; Jiang, Y. Visualizing Eigen/Zundel cations and their interconversion in monolayer water on metal surfaces. *Science* **2022**, *377*, 315-319.

(20) Pérez, C.; Neill, J. L.; Muckle, M. T.; Zaleski, D. P.; Peña, I.; López, J. C.; Alonso, J. L.; Pate, B. H. Water–water and water–solute interactions in microsolvated organic complexes. *Angew. Chem. Int. Ed.* **2015**, *54*, 979–982.

(21) Gong, X.; Heck, S.; Jelovina, D.; Perry, C.; Zinchenko, K.; Lucchese, R.; Wörner. H. J. Attosecond spectroscopy of size-resolved water clusters. *Nature* **2022**, *609*, 507-511.

(22) Li, W.; Quesada-Moreno, M. M.; Pinacho, P.; Schnell, M. Unlocking the water trimer loop: Isotopic study of benzophenone-$(H_2O)_{1\text{-}3}$ clusters with rotational spectroscopy. *Angew. Chem. Int. Ed.* **2021**, *60*, 5323-5330.

(23) Pribble, R. N.; Zwier, T. S. Size-specific infrared spectra of benzene-$(H_2O)_n$ clusters (n = 1 through 7): Evidence for noncyclic $(H_2O)_n$ structures. *Science* **1994**, *265*, 75-79.

(24) Gruenloh, C. J.; Carney, J. R.; Arrington, C. A.; Zwier, T. S.; Fredericks, S. Y.; Jordan, K. D. Infrared spectrum of a molecular ice cube: The S_4 and D_{2d} water octamers in benzene-$(water)_8$. *Science* **1997**, *276*, 1678-1681.

(25) Tabor, D. P.; Kusaka, R.; Walsh, P. S.; Sibert, E. L.; Zwier, T. S. Isomer-specific spectroscopy of benzene-$(H_2O)_n$, n = 6, 7: Benzene's role in reshaping water's three-dimensional networks. *J. Phys. Chem. Lett.* **2015**, *6*, 1989-1995.

(26) Zhang, B.; Yu, Y.; Zhang, Y.; Jiang, S.; Li, Q.; Hu, H.; Li, G.; Zhao, Z.; Wang, C.; Xie, H.; Zhang, W.; Dai, D.; Wu, G.; Zhang, D.; Jiang, L.; Li, J.; Yang, X. Infrared spectroscopy of neutral water clusters at finite temperature: Evidence for a noncyclic pentamer. *Proc. Nat. Acad. Sci.* USA **2020**, *117*, 15423-15428.

(27) Li, G.; Zhang, Y.; Li, Q.; Wang, C.; Yu, Y.; Zhang, B.; Hu, H.; Zhang, W.; Dai, D.; Wu, G.; Zhang, D.; Li, J.; Yang, X.; Jiang, L. Infrared spectroscopic study of hydrogen bonding topologies in the smallest ice cube. *Nat. Commun*. **2020**, *11*, 5449.

(28) Gordy, W.; Cook, L. R. *Microwave Molecular Spectra*, 3rd ed.; John Wiley & Sons, New York, 1984.

(29) Grabow, J. U.; Caminati, W. Microwave spectroscopy: experimental techniques. In *Frontiers of Molecular Spectroscopy*, Elsevier, 2009; pp 383-454.

(30) Caminati, W.; Grabow, J-U.; Advancements in microwave spectroscopy. *In Frontiers and advances in molecular spectroscopy*, Elsevier, **2018**, 569-598.

(31) Pate, B. H.; Evangelisti, L.; Caminati, W.; Xu, Y.; Thomas, J.; Patterson, D.; Perez, C.; Schnell, M. Quantitative chiral analysis by molecular rotational spectroscopy. In *Chiral Analysis*, Elsevier, 2018; pp 679-729.

(32) Kraitchman, J. Determination of molecular structure from microwave spectroscopic data. *Am. J. Phys.* **1953**, *21*,17-24.

(33) Brown, G. G.; Dian, B. C.; Douglass, K. O.; Geyer, S. M.; Shipman, S. T.; Pate, B. H. A broadband Fourier transform microwave spectrometer based on chirped pulse excitation. *Rev. Sci. Instrum.* **2008**, *79*, 053103.

(34) Barratt, P. G.; Field, R. W. Perspective: The first ten years of broadband chirped pulse Fourier transform microwave spectroscopy. *J. Chem. Phys.* **2016**, *144*, 200901.

(35) Pérez, C.; Muckle, M. T.; Zaleski, D. P.; Seifert, N. A.; Temelso, B.; Shields, G. C.; Kisiel, Z.; Pate. B. H. Structures of cage, prism, and book isomers of water hexamer from broadband rotational spectroscopy. *Science* **2012**, 336, 897-901.

(36) Richardson, J. O.; Pérez, C.; Lobsiger, S.; Reid, A. A.; Temelso, B.; Shields, G. C.; Kisiel, Z.; Wales, D. J.; Pate, B. H.; Althorpe, S. C. Concerted hydrogen-bond breaking by quantum tunneling in the water hexamer prism. *Science* **2016**, *351*, 1310-1313.

(37) Pérez, C.; Lobsiger, S.; Seifert, N. A.; Zaleski, D. P.; Temelso, B.; Shields, G. C.; Kisiel, Z.; Pate, B. H. Broadband Fourier transform rotational spectroscopy for structure determination: The water heptamer. *Chem. Phys. Lett.* **2013**, *571*, 1-15.

(38) Pérez, C.; Zaleski, D. P.; Seifert, N. A.; Temelso, B.; Shields, G. C.; Kisiel, Z.; Pate, B. H. Hydrogen bond cooperativity and the three-dimensional structures of water nonamers and decamers. *Angew. Chem. Int. Ed*. **2014**, *53*, 14368-14372.

(39) Steber, A. L.; Pérez, C.; Temelso, B.; Shields, G. C.; Rijs, A. M.; Pate, B. H.; Kisiel, Z.; Schnell, M. Capturing the elusive water trimer from the stepwise growth of water on the surface of the polycyclic aromatic hydrocarbon acenaphthene. *J. Phys. Chem. Lett.* **2017**, *8*, 5744–5750.

(40) Evangelisti, L.; Pérez, C.; Temelso, B.; Shields, G. C.; Pate, B. Characterization of ammonia-water clusters by broadband rotational spectroscopy. In Abstracts & Presentations, *2016 International Symposium on Molecular Spectroscopy*, Urbana-Champaign, IL. https://www.ideals.illinois.edu/items/97918.

(41) Li, W.; Pinacho, P.; Quesada-Moreno, M. M.; Schnell, M. The competition and cooperativity of non-covalent bonds in benzophenone-$(H_2O)_{1,2,3}$ clusters revealed by broadband microwave spectroscopy. In Abstracts & Presentations, *2019 International Symposium on Molecular Spectroscopy*, Urbana-Champaign, IL. https://www.ideals.illinois.edu/items/113359.

(42) Burevschi, E.; Chrayteh, M.; Loru, D.; Dréan, P.; Sanz, M. E. Multiple water configurations in fenchone $\cdots$ $(H_2O)_{1\text{-}6}$ hydrates revealed by rotational spectroscopy. In Book of Abstracts, 2022 *International Symposium on Molecular Spectroscopy*, Urbana-Champaign, IL; Paper WM03.

(43) Sun, W.; Schnell, M. Microhydrated 3-Methyl-3-oxetanemethanol: Evolution of the hydrogen-bonding network from chains to cubes. *Angew. Chem. Int. Ed.* **2022**, *61*, e202210819.

(44) Schmitz, D.; Shubert, V. A.; Betz, T.; Schnell, M. Multi-resonance effects within a single chirp in broadband rotational spectroscopy: The rapid adiabatic passage regime for benzonitrile. *J. Mol. Spectrosc.* **2012**, *280*, 77–84.

(45) Plusquellic, D. F. JB95 Spectral Fitting Program, NIST, Gaithersburg. https://www.nist.gov/services-resources/software/jb95-spectral-fitting-program (accessed 2022-12-24).

(46) Kisiel, Z.; Pszczolkowski, L.; Medvedev, I. R.; Winnewisser, M.; De Lucia, F. C.; Herbst, E. Rotational spectrum of trans–trans diethyl ether in the ground and three excited vibrational states. *J. Mol. Spectrosc.* **2005**, *233*, 231-243.

(47) Watson, J. K. G. Aspects of quartic and sextic centrifugal effects on rotational energy levels. In *Vibrational Spectra and Structure*. Durig, J. R., Ed.; Elsevier: New York/Amsterdam, 1977; vol. *6*, pp 1–89.

(48) Pickett, H. M. The fitting and prediction of vibration-rotation spectra with spin interactions. *J. Mol. Spectrosc.* **1991**, *148*, 371-377.

(49) Kisiel, Z. Least-squares mass-dependence molecular structures for selected weakly bound intermolecular clusters. *J. Mol. Spectrosc.* **2003**, *218*, 58-67.
(50) Watson, J. K. G; Roytburg, A.; Ulrich. W. Least-squares mass-dependence molecular structures. *J. Mol. Spectrosc.* **1999**, *196*, 102-119.
(51) Pracht, P.; Bohle, F.; Grimme, S. Automated exploration of the low-energy chemical space with fast quantum chemical methods. *Phys. Chem. Chem. Phys.* **2020**, *22*, 7169-7192.
(52) Grimme, S.; Antony, J.; Ehrlich, S.; Krieg, H. A consistent and accurate ab initio parametrization of density functional dispersion correction (DFT-D) for the 94 elements H-Pu. *J. Chem. Phys.* **2010**, *132*, 154104.
(53) Neese, F. Orca Version 4.0.1, *WIREs Comput. Mol. Sci.* **2012**, *2*, 73-78.
(54) Johnson, E. R.; Keinan, S.; Mori-Sánchez, P.; Contreras-García, J.; Cohen, A. J.; Yang, W. Revealing noncovalent interactions. *J. Am. Chem. Soc*. **2010**, *132*, 6498-6506.
(55) Lu, T.; Chen, F. Multiwfn: A multifunctional wavefunction analyzer, *J. Comput. Chem.* **2012**, *33*, 580-592.
(56) Pettersen, E. F.; Goddard, T. D.; Huang, C. C.; Couch, G. S.; Greenblatt, D. M.; Meng, E. C.; Ferrin. T. E. UCSF Chimera—A visualization system for exploratory research and analysis. *J Comput. Chem.* **2004**, *25*, 1605-1612.
(57) Desyatnyk, O.; Pszczółkowski, L.; Thorwirth, S.; Krygowski, T. M.; Kisiel, Z. The rotational spectra, electric dipole moments and molecular structures of anisole and benzaldehyde. *Phys. Chem. Chem. Phys*. **2005**, 7, 1708-1715.
(58) Li, W.; Maris, A.; Calabrese, C.; Usabiaga, I.; Geppert, W. D.; Evangelisti, L.; Melandri, S. Atmospherically relevant acrolein–water complexes: Spectroscopic evidence of aldehyde hydration and oxygen atom exchange. *Phys. Chem. Chem. Phys.* **2019**, *21*, 23559-23566.
(59) Evangelisti, L.; Caminati, W. Internal dynamics in complexes of water with organic molecules. Details of the internal motions in tert-butylalcohol–water. *Phys. Chem. Chem. Phys.* **2010**, *12*, 14433-14441.
(60) Pugliano, N.; Saykally, R. J. Measurement of quantum tunneling between chiral isomers of the cyclic water trimer. *Science* **1992**, *257*, 1937-1940.
(61) Liu, K.; Brown, M. G.; Cruzan, J. D.; Saykally, R. J. Vibration-rotation tunneling spectra of the water pentamer: Structure and dynamics. *Science* **1996**, *271*, 62-64.
(62) Favero, L. B.; Li, W.; Spadini, G.; Caminati, W. Ring puckering splitting and structure of indan. *J. Mol. Spectrosc.* **2015**, *316* 45-48.
(63) Cruzan, J. D.; Braly, L. B.; Liu, K.; Brown, M. G.; Loeser, J. G.; Saykally, R. J. Quantifying hydrogen bond cooperativity in water: VRT spectroscopy of the water tetramer. *Science* **1996**, *271*, 59-62.
(64) Watanabe, T.; Ebata, T.; Tanabe, S.; Mikami, N. Size selected vibrational spectra of phenol-$(H_2O)_n$ (n=1-4) clusters observed by IR-UV double resonance and stimulated Raman-UV double resonance spectroscopies. *J. Chem. Phys.* **1996**, *105*, 408-419.
(65) Jacoby, C.; Roth, W.; Schmitt, M.; Janzen, C.; Spangenberg, D.; Kleinermanns, K. Intermolecular vibrations of phenol-$(H_2O)_{2\text{-}5}$ and phenol-$(D_2O)_{2\text{-}5\text{-}d1}$ studied by UV double-resonance spectroscopy and ab initio theory. *J. Phys. Chem. A* **1998**, *102*, 4471-4480.
(66) Janzen, C.; Spangenberg, D.; Roth, W.; Kleinermanns, K. Structure and vibrations of phenol $(H_2O)_{7,8}$ studied by infrared-ultraviolet and ultraviolet-ultraviolet double-resonance spectroscopy and ab initio theory. *J. Chem. Phys.* **1999**, *110*, 9898-9907.
(67) Pérez, C.; Steber, A. L.; Temelso, B.; Kisiel, Z.; Schnell, M. Water triggers hydrogen-bond-network reshaping in the glycoaldehyde dimer. *Angew. Chem. Int. Ed.* **2020**, *59*, 8401-8405.
(68) Liu, K.; Brown, M. G.; Carter, C.; Saykally, R. J.; Gregory, J. K.; Clary, D. C. Characterization of a cage form of the water hexamer. *Nature* **1996**, *381*, 501-503.
(69) Nauta K.; Miller R. E. Formation of cyclic water hexamer in liquid helium: The smallest piece of ice. *Science* **2000**, *287*, 293-295.
(70) Steinbach C.; Andersson, P.; Melzer, M.; Kazimirski, J. K.; Buck, U.; Buch, V. Detection of the book isomer from the OH-stretch spectroscopy of size selected water hexamers. *Phys. Chem. Chem. Phys.* **2004**, *6*, 3320-3324.

TOC Graphic